J. Fluid Mech. (2000), *vol.* 419, *pp.* 151–175. Printed in the United Kingdom

Trapped acoustic modes in aeroengine intakes with swirling flow

By A. J. COOPER AND N. PEAKE

Department of Applied Mathematics and Theoretical Physics, University of Cambridge, Silver Street, Cambridge, CB3 9EW, UK

(Received 17 November 1999)

A theoretical model of an aeroengine intake–fan system is developed in order to show the existence of acoustic resonance in the intake. In general this phenomenon can be linked to instabilities in aircraft engine inlets.

The model incorporates a slowly varying duct intake and accounts for the swirling flow downstream of the fan. The slow axial variation in cross-section gives rise to turning points where upstream-propagating acoustic modes are totally reflected into downstream-propagating modes. The effect of the swirling flow downstream can be to cut off a mode which is cut on upstream of the fan. It is shown that these two aspects of the flow, coupled with the effects of the fan (represented by an actuator disc), can lead to acoustic modes becoming trapped in the intake, thus giving rise to pure acoustic resonance.

A whole range of system parameters, such as axial, fan and swirl Mach numbers, which satisfy the conditions for resonance are identified. The effects of a stationary blade row behind the fan are also considered leading to a second family of resonant states. In addition we find resonance due to reflection of acoustic modes at the open (inlet) end of the duct.

1. Introduction

The continuing development of larger aeroengines and the wider range of conditions over which they are required to operate has created a number of urgent design issues. One concern is the possible excitation of fluid-dynamical and acoustic instabilities within the engine, which if allowed to develop can have potentially serious operational consequences, with the effect of compromising the (design) operating range of the engine. This would lead to significant degradation in performance and potentially necessitate costly engine redesign.

Here we address one such instability which is of considerable practical interest and concern, namely the aeroacoustic coupling between the intake geometry/flow and the fan, which can potentially be linked to flutter and/or rotating stall in the fan. This form of instability typically occurs in the mid-range of Mach numbers (0.3–0.6) and is a relatively low-frequency phenomenon (200–600 Hz) with acoustic wavelengths taking values of the order of the fan radius. In this paper a theoretical model is developed to predict the conditions for instability across a range of operating conditions (which may provide information that could be used at an early stage in the design process).

Variation in the cross-sectional shape of the nacelle is a crucial factor in generating instabilities, and our model therefore includes an axisymmetric duct which varies

slowly in the axial direction to represent the intake. In hard-walled ducts with varying cross-section, turning points can arise within the duct, corresponding to points where a mode changes from being cut on to cut off. Thus an upstream-propagating acoustic mode must be reflected into a downstream-propagating mode at a turning point. Swirling flow behind the fan can also play a role in generating the instability, since modes which are cut on ahead of the fan can be cut off by the mean swirl behind the fan, providing a potential mechanism for the reflection of incident acoustic waves at the fan. Thus the combination of swirling flow behind the fan and the existence of turning points upstream of the fan leads to the possibility of acoustic modes becoming trapped in the intake, giving rise to pure acoustic resonance and the development of a large-amplitude, saturated-state oscillation.

An actuator disc, a theoretical tool which provides jump conditions in flow properties, is used to represent the effect of the fan. Actuator discs have been used widely to represent blade rows in internal flows, and many applications are described in Horlock (1978). We will be concerned here only with modes of low azimuthal order, and for these modes it is believed that the actuator disc model is entirely adequate. Flow quantities, such as mass flow and radial velocity, are conserved on either side of the fan and provide boundary conditions which are applied across the actuator disc.

Various aspects related to this investigation have been considered previously. Work on acoustic flow in slowly varying ducts using the WKB technique has been carried out by Nayfeh, Shaker & Kaiser (1980) and Nayfeh & Telionis (1973). Howe & Liu (1977) have considered noise generation in an axisymmetric duct which varies in cross-sectional area, and Eversman & Astley (1981) and Astley & Eversman (1981) describe numerical work on general area variation. Recently Rienstra (1999) carried out an explicit multiple-scales analysis of a slowly varying cylindrical duct with mean flow. The question of resonance, however, particularly in view of the novel end condition provided by the fan, has not been addressed.

The effect of mean swirling flow in ducts on the propagation of small disturbances was first analysed by Kerrebrock (1977). This work has been extended by Golubev & Atassi (1995, 1996, 1998) who studied the effects of mean potential swirling flow, and a more general swirl profile defined in terms of rigid-body rotation and a free vortex, in annular ducts. This has also been considered by Tam & Auriault (1998). Using a normal-mode analysis, mean swirling flow was shown to couple acoustic and vorticity modes, and give rise to pressure-dominated nearly sonic waves and vorticity-dominated nearly convected modes.

There is a substantial body of work concerning the existence of trapped modes and the occurrence of acoustic resonance. Evans, Levitin & Vassiliev (1994) provided the first general existence proof for modes trapped by an obstacle in a two-dimensional waveguide. Subsequent work on mode trapping by obstacles in ducts is described in Evans & Linton (1994) and Linton & McIver (1998*a*, *b*). Also related is work on the existence of water-wave trapping by rigid bodies (see Evans & Linton 1991). Early work in the area of acoustic resonance and blade rows was undertaken by Parker (1966, 1967) where both theoretical prediction and experimental verification of trapped modes was obtained. Recently Woodley & Peake (1999*a*, *b*) investigated the existence of trapped acoustic modes in a system of twin blade rows, or cascades, which is related to acoustic resonance in aeroengine compressors. The importance of acoustic resonance from a practical viewpoint is reviewed by Parker & Stoneman (1989), which details other areas of the aeroengine where the effects of acoustic resonance may be significant.

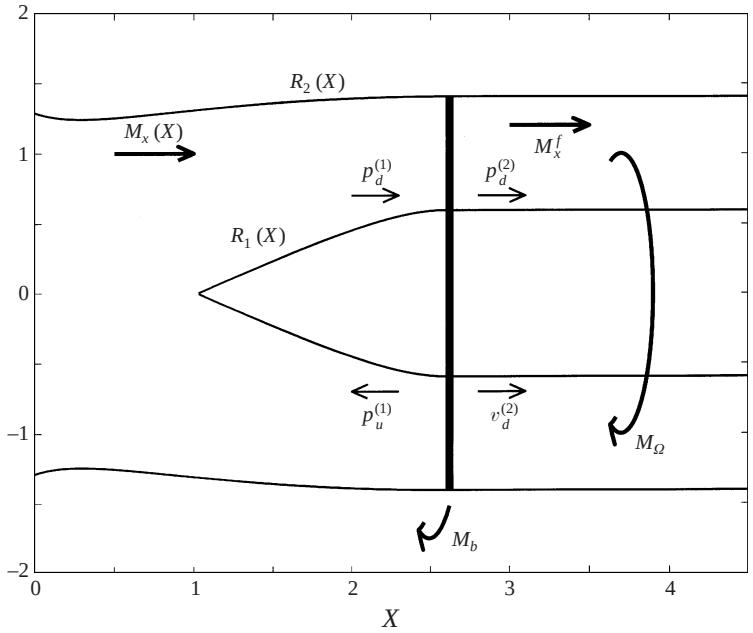

FIGURE 1. Schematic of duct–fan region. Upstream of the fan (located at $X_f = 2.619$) the duct is slowly varying with duct walls defined by $R_1(X), R_2(X)$. The mean flow is defined by an axial Mach number $M_x(X)$. Acoustic perturbations are represented by $p_u^{(1)}$ (upstream propagating) and $p_d^{(1)}$ (downstream propagating). Fan speed is expressed in terms of a blade Mach number M_b. Downstream of the fan the mean flow consists of uniform axial flow (M_x^f) and a rigid-body rotation (M_Ω). Downstream-propagating coupled acoustic-vorticity perturbations are represented by $p_d^{(2)}$ and $v_d^{(2)}$.

2. Modelling the intake–fan system

A clean axisymmetric aeroengine intake is represented by a cylindrical duct with slowly varying cross-section. The duct is hollow at the inlet and undergoes a transition to an annular duct as the fan is approached, thus modelling the presence of a spinner. The flow within the duct is taken to consist of a steady mean flow with unsteady acoustic perturbations. The steady flow into the duct is axisymmetric and governed by the compressible Euler equations with slow axial variation. The unsteady flow is then treated as a small linearized perturbation to the mean flow. A schematic of the intake–fan system and swirling flow region is shown in figure 1.

At the fan the duct is assumed to be locally parallel with uniform steady axial flow into the fan. Downstream of the fan the duct remains parallel and the mean flow has an additional swirling (azimuthal) component. The fan itself is modelled by an actuator disc which provides appropriate boundary (or jump) conditions, and couples the flow upstream and downstream of the fan. In the region upstream of the fan it is assumed that the steady flow is irrotational and that both upstream- and downstream-propagating acoustic modes exist. Behind the fan the swirl gives rise to coupled acoustic–vorticity modes (Golubev & Atassi 1998) and only those which propagate in the downstream direction are assumed to be present (this assumption will need to be relaxed when we include another blade row downstream).

The analysis of Rienstra (1999) for sound propagation in a slowly varying cylindrical duct is used to determine where acoustic modes are cut on and cut off upstream of

the fan. The variation in cross-sectional area of the duct means that turning points can exist within the inlet duct, where an upstream-propagating cut-on mode is totally reflected into a downstream-propagating cut-on mode. Following Golubev & Atassi (1998) it is shown here that a mode which is cut on at the fan can be cut off by the swirling flow behind it, so that at the fan an incident downstream-propagating mode may be reflected back into upstream-propagating modes. We therefore have the possibility of modes becoming trapped within the duct between the turning point location and the fan, generating pure acoustic resonance. The Rienstra analysis is used to determine the frequencies which give rise to turning points within the duct, and the actuator disc calculation, which couples the flow upstream and downstream of the fan, is then used to determine the parameters which allow trapped or resonant modes to exist.

Another mechanism for the possible containment of acoustic modes is the reflection of a cut-on mode at the open end of the duct. This case is also considered and uses reflection coefficients for the reflection of an incident acoustic mode at the open end of a cylindrical duct, which are calculated using the Wiener–Hopf technique (see Levine & Schwinger 1948). The presence of a stationary blade row (stator, or Outlet Guide Vanes) is also considered by the inclusion of a second actuator disc downstream which returns the steady flow to being purely axial.

3. Theory

3.1. *Slowly varying cylindrical duct*

Consider a hard-walled cylindrical duct, with cylindrical coordinate system (x, r, θ), which has slowly varying cross-section. In a study of the transmission of sound in a slowly varying duct, Rienstra (1999) used the method of multiple scales to account for the variation in duct shape, and that formulation is followed here. A small parameter ε is introduced to define a slow axial scale X, such that $X = \varepsilon x$ (ε is of the order of the axial slope of the duct walls). The inner radius of the duct, R_1, and the outer radius, R_2, are then defined as functions of X.

A nearly uniform mean flow of the form

$$\boldsymbol{V} = U(X, r; \varepsilon)\boldsymbol{e}_x + V(X, r; \varepsilon)\boldsymbol{e}_r \tag{1}$$

is assumed, and mean flow quantities are expanded in powers of ε as

$$U(X, r; \varepsilon) = U_0(X) + O(\varepsilon^2), \quad V(X, r; \varepsilon) = \varepsilon V_1(X, r) + O(\varepsilon^3), \tag{2}$$

$$P(X, r; \varepsilon) = P_0(X) + O(\varepsilon^2), \quad D(X, r; \varepsilon) = D_0(X) + O(\varepsilon^2), \quad C(X, r; \varepsilon) = C_0(X) + O(\varepsilon^2), \tag{3}$$

where P is the mean pressure, D the mean density and C the speed of sound. Throughout lengths are non-dimensionalized by R_m, the average of the inner and outer duct radii at the fan, velocities by a reference sound speed c_∞, density by ρ_∞ and pressure by $\rho_\infty c_\infty^2$. The leading-order terms U_0 and hence P_0, C_0, D_0 and V_1 are given exactly in Rienstra (1999). The local axial Mach number along the duct is given by $M_x(X) = U_0(X)/C_0(X)$.

The acoustic field is expressed in terms of a potential with slowly varying amplitude and axial and radial wavenumbers in the form

$$\phi(x, r, \theta, t; \varepsilon) = A(X, r; \varepsilon) \exp\left(\mathrm{i}\omega t - \mathrm{i}m\theta - \frac{\mathrm{i}}{\varepsilon}\int^X \mu(\xi)\mathrm{d}\xi\right). \tag{4}$$

By expanding the amplitude of the potential in powers of ε, such that

$$A(X, r; \varepsilon) = A_0(X, r) + \varepsilon A_1(X, r) + \cdots, \tag{5}$$

and equating like powers of ε, the leading-order amplitude, A_0, is determined by Rienstra in the form

$$A_0(X, r) = N(X) J_m(\alpha(X) r) + M(X) Y_m(\alpha(X) r), \tag{6}$$

where

$$\alpha^2 = \frac{\Lambda^2}{C_0^2} - \mu^2, \tag{7}$$

$$\Lambda = \omega - \mu U_0. \tag{8}$$

J_m and Y_m are mth-order Bessel functions of the first and second kinds respectively, and $N(X)$ and $M(X)$ are arbitrary functions. The radial eigenvalues $\alpha(X)$, and hence from (7) the axial wavenumbers $\mu(X)$, are found by applying the boundary conditions of zero radial velocity on the walls

$$\frac{\partial A_0}{\partial r} = 0 \quad \text{at} \quad r = R_1(X), R_2(X). \tag{9}$$

By eliminating $M(X)$ the following dispersion relation for $\alpha(X)$ is obtained:

$$J'_m(\alpha R_1) Y'_m(\alpha R_2) - J'_m(\alpha R_2) Y'_m(\alpha R_1) = 0, \tag{10}$$

where the prime denotes differentiation with respect to the argument. With $\alpha(X)$ determined, $M(X)$ and $N(X)$ are related by

$$M(X) = -N(X) \frac{J'_m(\alpha R_2)}{Y'_m(\alpha R_2)}, \tag{11}$$

which then leaves A_0 in terms of one arbitrary function of X.

From (7) it is clear that for each α there are two allowed values of μ, which give rise to upstream- (μ^-) and downstream- (μ^+) propagating waves. Modes with $\mathrm{Im}(\mu) = 0$ are referred to as cut on and those with $\mathrm{Im}(\mu) \neq 0$ as cut off. For a given m there are generally a finite number of cut-on modes and an infinite discrete set of cut-off (or evanescent) modes (these are non-propagating in the frame of reference moving with the mean axial velocity). A typical eigenvalue spectrum is shown in figure 2.

At the fan location ($x = x_f$, or equivalently $X = X_f$), the duct is assumed to be locally parallel, so that the solution there can be written as

$$\phi_m(x, r, \theta; t) = \sum_{n=1}^{\infty} \left\{ A^u_{mn} \mathrm{e}^{-\mathrm{i}\mu^-_{mn}(x - x_f)} + A^d_{mn} \mathrm{e}^{-\mathrm{i}\mu^+_{mn}(x - x_f)} \right\} C_m(\alpha_{mn} r) \mathrm{e}^{\mathrm{i}(\omega t - m\theta)}, \tag{12}$$

where A^u_{mn} and A^d_{mn} are coefficients of the upstream-and downstream-propagating waves respectively, and $C_m(z) = J_m(z) - \{J'_m(\alpha_{mn} r_t)/Y'_m(\alpha_{mn} r_t)\} Y_m(z)$, with $r_t = R_2(X_f)$; m and n are integers labelling the circumferential and radial modes respectively. From (7) the wavenumbers $\mu^{\pm}_{mn}$ at the fan are given by

$$\mu^{\pm}_{mn} = \frac{-k_0 M^f_x \pm \sqrt{k_0^2 - \alpha^2_{mn}(1 - M^{f2}_x)}}{1 - M^{f2}_x}, \tag{13}$$

where $k_0 = \omega / C_0(X_f)$ and $M^f_x = M_x(X_f)$ is the Mach number at the fan location.

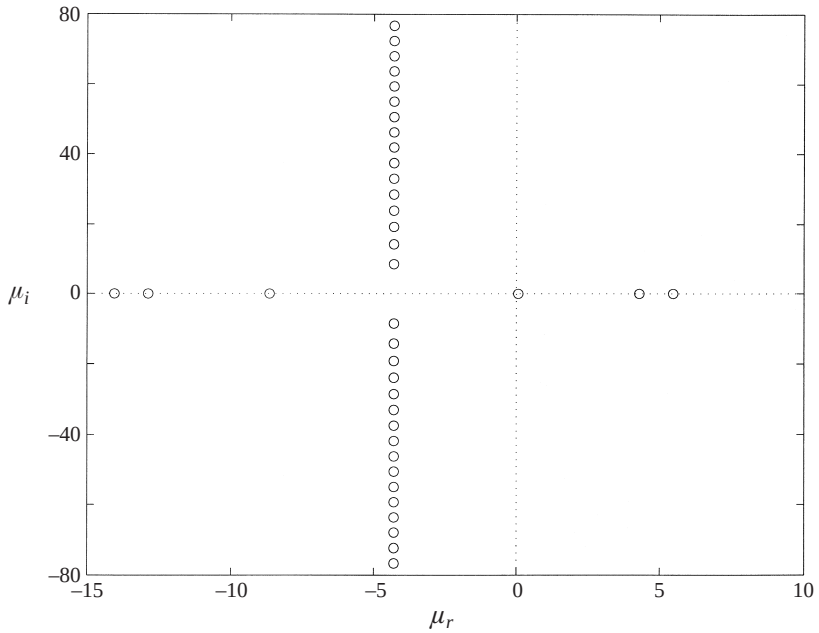

FIGURE 2. Eigenvalues μ_{mn} (pressure modes) for non-swirling flow with $m = 2$, $\omega = 8.16$, $M_x^f = 0.4292$, $r_h = 0.59488$, $r_t = 1.4046$. The single vorticity mode is located at 19.01 on the real axis.

3.2. *Uniform swirling flow*

Behind the fan the duct is taken to be a uniform cylindrical annulus of dimension $R_1(X_f) = r_h \leqslant r \leqslant r_t = R_2(X_f)$, with a swirling mean flow consisting of a uniform axial flow and rigid-body rotation such that

$$\boldsymbol{V} = U_0^f \boldsymbol{e}_x + \Omega r \boldsymbol{e}_\theta, \tag{14}$$

where $U_0^f = U_0(X_f)$. The mean density $D = \rho_0(r)$ satisfies

$$\frac{1}{\gamma - 1}\frac{\partial \rho_0}{\partial r} = \Omega^2 r, \tag{15}$$

where γ is the ratio of specific heats.

This type of mean swirling flow has been studied by Golubev & Atassi (1998) and Tam & Auriault (1998). Due to the presence of mean swirling flow behind the fan, the linearized Euler equations for small-amplitude perturbations to the three unsteady velocity components and pressure, (u_x, u_r, u_θ, p), form the set of coupled equations

$$\frac{1}{C_0^2}\left(\frac{\partial p}{\partial t} + U_0^f \frac{\partial p}{\partial x} + \Omega \frac{\partial p}{\partial \theta}\right) + \rho_0 \left(\frac{\partial u_x}{\partial x} + \frac{\partial u_r}{\partial r} + \frac{u_r}{r} + \frac{1}{r}\frac{\partial u_\theta}{\partial \theta}\right) + \frac{\partial \rho_0}{\partial r} u_r = 0, \tag{16}$$

$$\rho_0 \left(\frac{\partial u_x}{\partial t} + U_0^f \frac{\partial u_x}{\partial x} + \Omega \frac{\partial u_x}{\partial \theta}\right) = -\frac{\partial p}{\partial x}, \tag{17}$$

$$-\frac{\Omega^2 r}{C_0^2} p + \rho_0 \left(\frac{\partial u_r}{\partial t} + U_0^f \frac{\partial u_r}{\partial x} + \Omega \frac{\partial u_r}{\partial \theta} - 2\Omega u_\theta\right) = -\frac{\partial p}{\partial r}, \tag{18}$$

$$\rho_0 \left(\frac{\partial u_\theta}{\partial t} + U_0^f \frac{\partial u_\theta}{\partial x} + \Omega \frac{\partial u_\theta}{\partial \theta} + 2\Omega u_r\right) = -\frac{1}{r}\frac{\partial p}{\partial \theta}. \tag{19}$$

The perturbation velocity $\boldsymbol{u} = (u_x, u_r, u_\theta)$ is decomposed into potential and vortical parts such that

$$\boldsymbol{u} = \nabla\phi + \boldsymbol{a}, \tag{20}$$

and the pressure perturbation is then expressed solely in terms of the potential

$$p = -\rho_0 \left(\frac{\partial}{\partial t} + \boldsymbol{V} \cdot \nabla \right) \phi. \tag{21}$$

Following Golubev & Atassi (1998) a normal-mode analysis is used to express the vortical velocity and potential in the form

$$\{a_x, a_r, a_\theta, \phi\}(x, r, \theta; t) = \int_{-\infty}^{\infty} \sum_{m=-\infty}^{\infty} \sum_{n=1}^{\infty} \{X_{mn}(r), R_{mn}(r), T_{mn}(r), \phi_{mn}(r)\} \times \exp\{\mathrm{i}(\omega t - m\theta - k_{mn}(x - x_f))\} \, \mathrm{d}\omega, \tag{22}$$

and since the problem is linear each Fourier component can be considered separately. The pressure modes are given by

$$p_{mn}(r) = -\mathrm{i}\rho_0(r) \Lambda_{mn} \phi_{mn}(r), \tag{23}$$

where

$$\Lambda_{mn} = \omega - k_{mn} U_0^f - m\Omega. \tag{24}$$

Using the expansion in (22), equations (16)–(19) become

$$\frac{\partial^2 \phi_{mn}(r)}{\partial r^2} + \left(\frac{1}{r} + \frac{1}{\rho_0} \frac{\partial \rho_0}{\partial r} \right) \frac{\partial \phi_{mn}(r)}{\partial r} + \left(\frac{\Lambda_{mn}^2}{C_0^2} - k_{mn}^2 - \frac{m^2}{r^2} \right) \phi_{mn}(r) + \left(\frac{1}{r} + \frac{1}{\rho_0} \frac{\partial \rho_0}{\partial r} \right) R_{mn}(r) + \frac{\partial R_{mn}(r)}{\partial r} - \frac{\mathrm{i}m}{r} T_{mn}(r) - \mathrm{i}k_{mn} X_{mn}(r) = 0, \tag{25}$$

$$\Lambda_{mn} X_{mn}(r) = 0, \tag{26}$$

$$\Lambda_{mn} R_{mn}(r) + 2\mathrm{i}\Omega T_{mn}(r) + 2\Omega \frac{m}{r} \phi_{mn}(r) = 0, \tag{27}$$

$$\Lambda_{mn} T_{mn}(r) - 2\mathrm{i}\Omega R_{mn}(r) - 2\mathrm{i}\Omega \frac{\partial \phi_{mn}(r)}{\partial r} = 0. \tag{28}$$

When $\Omega \neq 0$ the presence of Coriolis forces prevents the existence of the purely convected solution given by $\Lambda_{mn} = 0$, so that we must have $X_{mn}(r) = 0$ from (26). As in Golubev & Atassi (1998) the remaining coupled equations are written in the form of a generalized eigenvalue problem

$$\boldsymbol{B}\,\boldsymbol{\Upsilon} = k_{mn}\,\boldsymbol{\Upsilon}, \tag{29}$$

where $\boldsymbol{\Upsilon} = [\phi_{mn}, \eta_{mn}, R_{mn}, T_{mn}]$ and $\eta_{mn} = k_{mn}\{1 - (U_0^f/C_0)^2\}\phi_{mn}$. The system of equations in (29) are solved numerically using a Chebyshev spectral-collocation method as in Khorrami (1991), with boundary conditions

$$\frac{\partial \phi_{mn}}{\partial r} + R_{mn} = 0 \quad \text{at} \quad r_h, r_t. \tag{30}$$

Since the presence of swirl couples the potential and vorticity equations, the eigenvalue relation produces two distinct sets of eigenvalues, and the corresponding eigenvectors are coupled acoustic–vorticity modes. One set of eigenmodes propagates with phase speeds close to the speed of sound and is sustained by compressibility

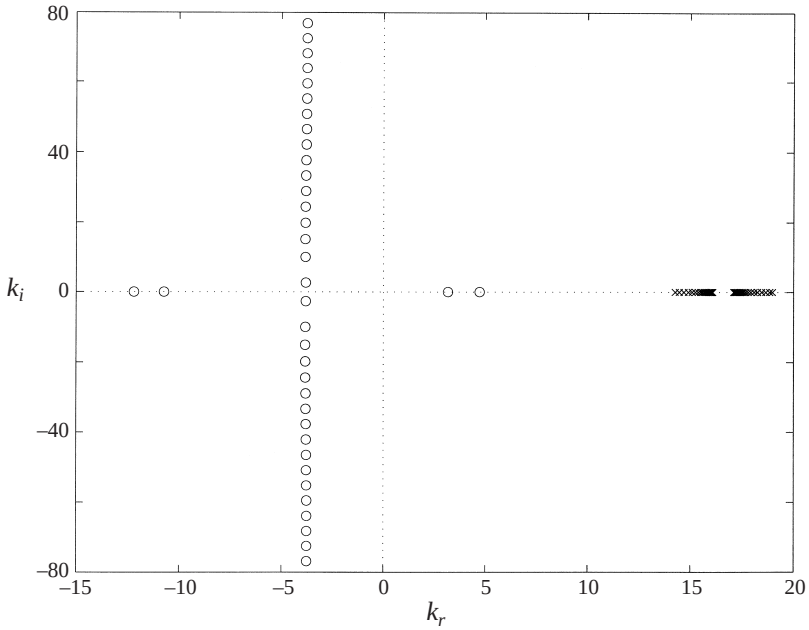

FIGURE 3. Eigenvalues k_{mn} for swirling flow with $m = 2$, $\omega = 8.16$, $M_x^f = 0.4292$, $M_\Omega = 0.525$, $r_h = 0.59488$, $r_t = 1.4046$. Circles denote pressure-dominated modes and crosses the rotational (vorticity-dominated) modes.

effects. This set is referred to by Golubev & Atassi (1998) as pressure-dominated modes, and consists of upstream- and downstream-propagating cut-on modes and an infinite discrete set of cut-off modes. The second set of eigenmodes is nearly convected, vorticity dominated and often referred to as rotational modes. This family of eigenmodes consists of two branches of eigenvalues (left and right) which asymptotically approach a singular point (given by $\Lambda_{mn} = 0$) corresponding to pure convection. A typical eigenvalue spectrum is shown in figure 3. By comparing figures 2 and 3 it can be seen that some of the modes which are cut on in the absence of mean swirl become cut off when $\Omega \neq 0$. It will be seen that it is this effect which is crucial in generating acoustic resonance in the intake.

At higher values of Ω the numerical scheme cannot resolve accurately all of the rotational modes and produces spurious roots which change value with the number of collocation points used. Since these modes are maintained by mean swirl (and not compressibility effects), they are determined by assuming constant density. This approximation is supported by Tam & Auriault (1998) who demonstrated that compressibility effects had only a minor influence on these modes. The pressure-dominated modes are determined throughout by solving the full set of equations. This produces a robust numerical scheme for determining all the eigenvalues and eigenvectors.

The velocities and pressure are expressed as

$$u_r = \sum_\tau \sum_{n=1}^{\infty} A_n^\tau \left\{ \frac{\partial \phi_n^\tau}{\partial r} + R_n^\tau \right\}, \tag{31}$$

$$u_\theta = \sum_\tau \sum_{n=1}^{\infty} A_n^\tau \left\{ \frac{-\mathrm{i}m\phi_n^\tau}{r} + T_n^\tau \right\}, \tag{32}$$

$$u_x = \sum_{\tau} \sum_{n=1}^{\infty} A_n^{\tau} \{-\mathrm{i}k_n^{\tau} \phi_n^{\tau}\}, \tag{33}$$

$$p = \sum_{\tau} \sum_{n=1}^{\infty} A_n^{\tau} \{-\mathrm{i}\Lambda_n^{\tau} \phi_n^{\tau}\}, \tag{34}$$

with a factor $\exp\{\mathrm{i}(\omega t - m\theta) - \mathrm{i}k_n^{\tau}(x - x_f)\}$ understood throughout. $\sum_{\tau}$ is used to denote the sum over the modes p, l and r, where superscript p denotes the pressure-dominated solution and superscripts l and r the left- and right-hand branches respectively of the rotational modes. The subscript m has been dropped for clarity.

3.3. *Actuator disc representation of the fan*

The rotating fan is modelled by placing an actuator disc inside the duct at $x = x_f$, which turns the flow and simulates jump conditions in flow properties. The unknown constants in the two flow regions are related through the jump conditions across the disc, corresponding to conservation of mass flow, conservation of radial velocity, conservation of rothalpy (total enthalpy in relative frame) and the Kutta condition of smooth flow at each trailing edge.

The region upstream of the fan is denoted region 1, and that downstream of the fan region 2. It is assumed that there exist incident acoustic waves and possible upstream-reflected waves in region 1, and in region 2 there may exist downstream-propagating acoustic-type waves and nearly convected vorticity-dominated waves. Using the notation in figure 1 (i.e. superscripts (1) and (2) to denote the unsteady flow fields in regions 1 and 2 respectively) the (linearized) mass and radial velocity jump conditions at the actuator disc are

$$\frac{M_x^f p^{(1)}}{C_0(X_f)} + D_0(X_f) u_x^{(1)} = \frac{M_x^f p^{(2)}}{C_0} + \rho_0 u_x^{(2)}, \tag{35}$$

$$u_r^{(1)} = u_r^{(2)}. \tag{36}$$

If the fan rotates with angular frequency W, then the rothalpy I is defined as

$$I = \left(\frac{\gamma}{\gamma - 1}\right) \frac{p}{\rho} + \tfrac{1}{2}\left\{V_x^2 + V_r^2 + (V_\theta - rW)^2\right\} - \tfrac{1}{2} r^2 W^2, \tag{37}$$

where (V_x, V_r, V_θ) is the total velocity field. The linearized jump condition expressing conservation of rothalpy then becomes

$$\frac{p^{(1)}}{D_0(X_f)} + C_0(X_f)\{M_x^f u_x^{(1)} - r M_b u_\theta^{(1)}\} = \frac{p^{(2)}}{\rho_0} + C_0\{M_x^f u_x^{(2)} + r(M_\Omega - M_b) u_\theta^{(2)}\}, \tag{38}$$

where $M_\Omega = \Omega R_m / (C_0(X_f) c_\infty)$ is the swirl Mach number, and $M_b = W R_m / (C_0(X_f) c_\infty)$ is the fan, or blade, rotational Mach number at the duct mean radius. The Kutta condition states that both the steady and unsteady flows must be aligned with the blades at the trailing edges. If the blades are inclined at an angle α to the axial flow at the trailing edge, then

$$\tan\alpha = \frac{r(M_\Omega - M_b)}{M_x^f} = \frac{u_\theta^{(2)}}{u_x^{(2)}}, \tag{39}$$

which leads to the condition

$$M_x^f u_\theta^{(2)} = r(M_\Omega - M_b) u_x^{(2)}. \tag{40}$$

Using the solution (12) for region 1 and the solutions (31)–(34) in region 2, the conditions at the actuator disc are expressed in terms of Bessel functions, unknown coefficients and system parameters. For example, the mass flow condition (35) becomes

$$\sum_n (Q_n^- A_n^u + Q_n^+ A_n^d) C_m(\alpha_n r) = \sum_n q_n^p A_n^p \phi_{mn}^p(r) + q_n^l A_n^l \phi_{mn}^l(r) + q_n^r A_n^r \phi_{mn}^r(r), \tag{41}$$

where

$$Q_n^\pm = -\mathrm{i} M_x^f \left\{ \frac{\omega}{C_0(X_f)} - M_x^f k_n^\pm \right\} - \mathrm{i} k_n^\pm D_0(X_f), \tag{42}$$

$$q_n^\tau = -\mathrm{i} M_x^f \frac{\Lambda_n^\tau}{C_0} - \mathrm{i} k_n^\tau \rho_0. \tag{43}$$

This can be transformed into a matrix equation by multiplying both sides by $rC_m(\alpha_j r)$, integrating from r_h to r_t, and using the identity

$$\begin{aligned} \int r C_m(\alpha_j r) C_m(\alpha_n r) \mathrm{d}r &= \frac{1}{2}\left(r^2 - \frac{m^2}{\alpha_j^2}\right) C_m^2(\alpha_j r) \quad \text{if} \quad j = n \\ &= 0 \qquad\qquad\qquad\qquad\quad \text{if} \quad j \neq n. \end{aligned}$$

The matrix equation resulting from (41) is

$$\boldsymbol{R}(\boldsymbol{Q}^- \boldsymbol{A}^u + \boldsymbol{Q}^+ \boldsymbol{A}^d) = \boldsymbol{H}^p \boldsymbol{A}^p + \boldsymbol{H}^l \boldsymbol{A}^l + \boldsymbol{H}^r \boldsymbol{A}^r, \tag{44}$$

where $\boldsymbol{A} = [A_1, A_2, \ldots]$ for each set of coefficients. The matrices $\boldsymbol{R}, \boldsymbol{Q}^\pm$ and $\boldsymbol{q}^\tau$ are diagonal with (no summation over repeated suffices)

$$R_{jj} = \left[\frac{1}{2}\left(r^2 - \frac{m^2}{\alpha_j^2}\right) C_m^2(\alpha_j r)\right]_{r_h}^{r_t}, \tag{45}$$

$$Q_{jj}^\pm = Q_j^\pm, \tag{46}$$

$$q_{jj}^\tau = q_j^\tau, \tag{47}$$

and

$$H_{jn}^p = \int_{r_h}^{r_t} r C_m(\alpha_j r) \phi_{mn}^p(r) q_n^p \mathrm{d}r, \tag{48}$$

with $\boldsymbol{H}^l$ and $\boldsymbol{H}^r$ defined in a similar manner.

Matrix equations for the remaining three conditions are formed by applying the same process to (36), (38) and (40), and can be written as

$$(\boldsymbol{S}^- \boldsymbol{A}^u + \boldsymbol{S}^+ \boldsymbol{A}^d) = \boldsymbol{B}^p \boldsymbol{A}^p + \boldsymbol{B}^l \boldsymbol{A}^l + \boldsymbol{B}^r \boldsymbol{A}^r, \tag{49}$$

$$\boldsymbol{R}(\boldsymbol{A}^u + \boldsymbol{A}^d) = \boldsymbol{P}^p \boldsymbol{A}^p + \boldsymbol{P}^l \boldsymbol{A}^l + \boldsymbol{P}^r \boldsymbol{A}^r, \tag{50}$$

$$0 = \boldsymbol{V}^p \boldsymbol{A}^p + \boldsymbol{V}^l \boldsymbol{A}^l + \boldsymbol{V}^r \boldsymbol{A}^r. \tag{51}$$

The resulting set of four simultaneous equations is manipulated to eliminate $\boldsymbol{A}^p, \boldsymbol{A}^l$ and $\boldsymbol{A}^r$, leaving a condition relating the amplitudes of the upstream-propagating modes ahead of the fan, $\boldsymbol{A}^u$, and the amplitudes of the downstream-propagating modes ahead of the fan, $\boldsymbol{A}^d$, which can be expressed in the form

$$\boldsymbol{A}^u = \boldsymbol{M} \boldsymbol{A}^d, \tag{52}$$

so that $\boldsymbol{M}$ can be thought of as a matrix of reflection coefficients. $\boldsymbol{A}^d$ contains only the coefficients of downstream-propagating cut-on modes, but both cut-on and cut-off

modes are included in the vector $\boldsymbol{A}^u$. This is because although the cut-off modes will decay as they propagate away from the fan, their contribution to the boundary conditions at the fan may be significant.

4. Acoustic resonance in the intake

We now define a condition which allows unforced acoustic resonance to exist. We concentrate on the case when there is, at most, a single cut-on mode at any point along the duct, and where there is precisely one cut-on mode at the fan face. This assumption is justified by the fact that the frequency ranges for which resonance may occur are characteristic of blade flutter, which is typically a relatively low-frequency phenomenon. Turning points can arise in the duct due to the slow changes in cross-sectional area, and are identified as points where the reduced axial wavenumber,

$$\sigma^{\pm} = \pm\sqrt{1 - C_0^2(1 - M_x^2)\frac{\alpha^2}{\omega^2}}, \tag{53}$$

passes through zero, to go from being purely real (cut on) to purely imaginary (cut off) or vice versa. Eigenvalue calculations for a slowly varying duct typically indicate the presence of one or two turning points within the inlet duct (possibly even more depending on flow conditions). For a given mass flux, the number and location of turning points depends on the frequency parameter ω. Figure 4 shows examples of how the reduced axial wavenumber $\sigma^{\pm}(X)$ varies with frequency for a given duct shape. A typical pattern is that a mode becomes cut on at the fan face and a single turning point is present upstream. As the frequency is increased the location of the turning point moves upstream, and increasing the frequency further gives rise to a second turning point between the open end of the duct and the first turning point. The two turning points then move towards each other, and finally merge to produce a mode which is cut on along the entire length of the duct. As the frequency is increased further a second mode becomes cut on at the fan.

In general, for any number of turning points, the condition relating the amplitudes of upstream- and downstream-propagating waves at the turning point nearest to the fan can be written

$$A^d(X_t) = RA^u(X_t), \tag{54}$$

where R is the reflection coefficient at the turning point and X_t is the location of the turning point. If the mode is cut on along the whole length of the duct then X_t is taken to be the location of the open end.

As the waves propagate along the duct their amplitudes $A^d(X)$ and $A^u(X)$ are related to the values at the turning point by some factor $T(X)$ as given in Rienstra (1999). Thus the right- and left-propagating waves at any position X downstream of the turning point are given by

$$A^d(X)\exp\left(-\frac{\mathrm{i}}{\varepsilon}\int_{X_t}^{X}\mu^+(y)\mathrm{d}y\right) = T(X)A^d(X_t)\exp\left(-\frac{\mathrm{i}}{\varepsilon}\int_{X_t}^{X}\mu^+(y)\mathrm{d}y\right), \tag{55}$$

$$A^u(X)\exp\left(-\frac{\mathrm{i}}{\varepsilon}\int_{X_t}^{X}\mu^-(y)\mathrm{d}y\right) = T(X)A^u(X_t)\exp\left(-\frac{\mathrm{i}}{\varepsilon}\int_{X_t}^{X}\mu^-(y)\mathrm{d}y\right). \tag{56}$$

At the actuator disc the duct is assumed to be locally parallel, and a local expansion of the above expressions about the fan position X_f produces expressions for the incoming and reflected waves which are in the same form as that used for the

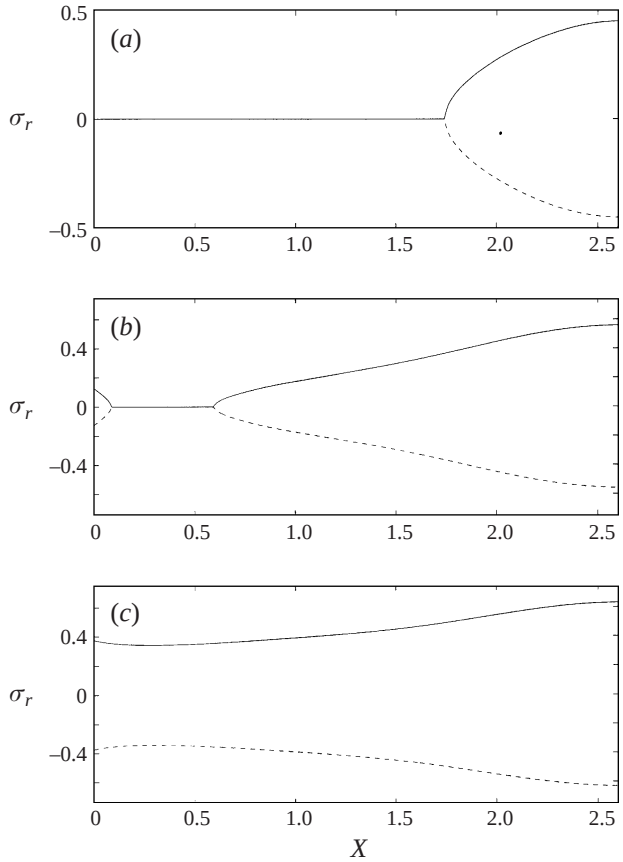

FIGURE 4. Variation in the real part of the reduced axial wavenumber, σ, along a slowly varying duct. Solid lines represent right-propagating modes and dashed lines left-propagating modes; modes are cut off when $\sigma_r = 0$. (*a*) $\omega = 2.0$, (*b*) $\omega = 2.2$, (*c*) $\omega = 2.4$.

actuator disc calculation. Therefore, at the fan location we have

$$A^d(X_f) = T(X_f)P^+A^d(X_t), \tag{57}$$

$$A^u(X_f) = T(X_f)P^-A^u(X_t), \tag{58}$$

where

$$P^{\pm} = \exp\left(-\frac{\mathrm{i}}{\varepsilon}\int_{X_t}^{X_f}\mu^{\pm}(y)\mathrm{d}y\right). \tag{59}$$

The expression relating right- and left-propagating modes at the fan is given by (52), which since we only consider a single incident (cut-on) mode, can be written as the scalar expression

$$A^u(X_f) = MA^d(X_f), \tag{60}$$

where $M = M_{11}$. Combining equations (54), (57), (58) and (60) gives

$$[1 - MP^+(P^-)^{-1}R]A^u(X_f) = 0, \tag{61}$$

and the resonance condition (i.e. the existence of a non-trivial solution for $A^u(X_f)$) is therefore

$$1 - MP^+(P^-)^{-1}R = 0, \tag{62}$$

or

$$M = \frac{1}{R}\exp\left(-\frac{\mathrm{i}}{\varepsilon}\int_{X_t}^{X_f}[\mu^-(y)-\mu^+(y)]\mathrm{d}y\right). \tag{63}$$

In general, a necessary condition for resonance to occur is that $|M| = |1/R|$. For a single turning point the reflection coefficient is $R = \exp(\mathrm{i}\pi/2)$, so that the upstream-propagating wave is totally reflected at the turning point. This $\pi/2$ phase jump between incident and reflected waves is of course characteristic of a ray caustic, and can be derived by considering an inner region around the turning point in which the wave amplitude $A_0(X)$ satisfies Airy's equation in a familiar way – see Rienstra & Hirschberg (1999) for details. The necessary condition for resonance in this particular case is that the modulus of M be equal to unity.

Once the parameters which give $|M| = 1$ have been determined, the phases in (63) are matched by an infinite set of values for ε as follows. If $M = \mathrm{e}^{\mathrm{i}\theta}$, then from (63)

$$\varepsilon = \frac{\displaystyle\int_{X_t}^{X_f}[\mu^-(y)-\mu^+(y)]\mathrm{d}y}{-\theta - \tfrac{1}{2}\pi \pm 2j\pi}, \qquad j = 0, 1, \ldots. \tag{64}$$

Each value of ε corresponds to a different duct shape, with ε being a measure of the axial slope of the duct walls, and each of these ducts will exhibit resonance in the parameter ranges which give $|M| = 1$.

If there is more than one cut-on mode upstream of the fan, then (61) becomes a matrix equation with $\boldsymbol{P}^{\pm}$ and $\boldsymbol{R}$ diagonal matrices of order n, where n is the number of cut-on modes. For the matrix equation the condition for resonance requires that the matrix $[\boldsymbol{I} - \boldsymbol{M}\boldsymbol{P}^{+}(\boldsymbol{P}^{-})^{-1}\boldsymbol{R}]$ be singular. Generally multiple cut-on modes occur at frequencies higher than those for which flutter typically occurs, and this regime will therefore not be considered further.

5. Results

The duct shape for the calculations is that used by Rienstra (1999), a CFM56-inspired turbofan engine, but with lengths non-dimensionalized here using the average duct radius at the fan. The duct is defined by

$$R_2(X) = 1.309\left\{1.073 - 0.198\left(1-\frac{X}{L}\right)^2 + 0.109\exp\left(-\frac{11X}{L}\right)\right\}, \tag{65}$$

$$R_1(X) = \max\left[0, 1.309\left\{0.689 - \sqrt{0.055 + 1.131\left(1-\frac{X}{L}\right)^2}\right\}\right], \tag{66}$$

$$0 \leqslant X \leqslant L, \quad L = 2.619,$$

and is shown in figure 5(*a*). A specified cross-sectional mass flux πF and stagnation enthalpy $E = 2.5419$ define the axial Mach number profile. This is shown in figure 5(*b*) for $F = 0.5$ and $F = 0.65$.

Fan flutter generally occurs for low-order azimuthal modes, and so the existence of acoustic resonance was investigated for values of $m = 2, 3, 4, 5$. For each value of m, frequency ranges across which single and double turning points arise, and those which give a single mode cut on along the length of the duct, were obtained. These

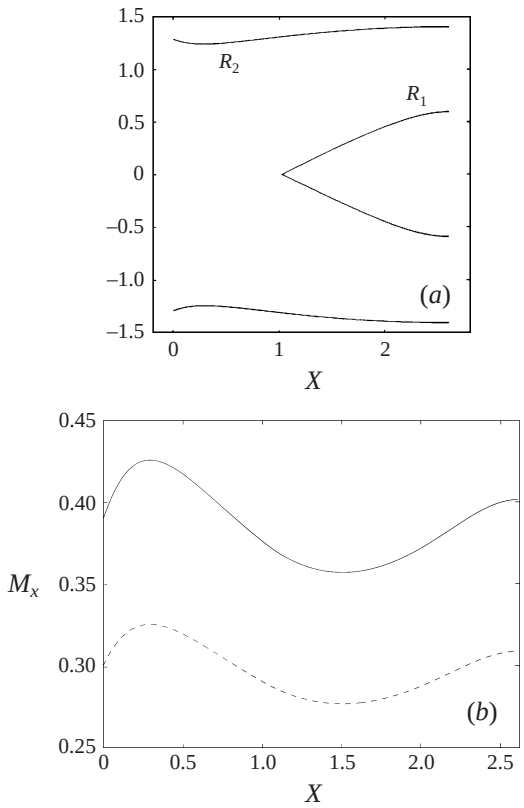

FIGURE 5. (*a*) Duct shape used in calculations; (*b*) variation in Mach number M_x along the duct for $F = 0.65$ ($M_x^I = 0.4015$) (solid line) and $F = 0.5$ ($M_x^I = 0.3089$) (dashed line).

frequency bands are given in figure 6 and show that the frequencies increase with increasing mode number m.

The actuator disc reflection coefficient M appearing in (60) is a function of $R_2(X_f)$, $R_1(X_f), M_x^I$, ω, M_b and M_Ω. The first three of these parameters are fixed for a given duct shape and axial mass flux. This leaves three free parameters which can be adjusted to satisfy the necessary resonance condition $|M| = 1$. Using the frequency ranges in figure 6, planes in (ω, M_b, M_Ω) parameter space are calculated which satisfy this condition, and thus potentially give rise to acoustic resonance. Calculations were carried out for swirl Mach numbers in the range $M_\Omega = 0.15 - 0.65$, and the solution planes are shown in figure 7. Several features are to be noted, the first being that for a fixed value of swirl Mach number M_Ω, higher values of the fan rotational Mach number M_b are required in order to satisfy the resonance condition as the frequency is increased in each band, and this increase is more pronounced for smaller values of m. As m is increased the planes lie at successively lower values of M_b, so that the minimum value of M_b satisfying the resonance condition occurs for the lowest frequency in the range for $m = 5$, and when $M_\Omega = 0.65$. (In the calculation of the matrix $\boldsymbol{M}$, results were found to converge when four or more modes were included.) Changes in mass flux, or axial Mach number, are found to alter the frequency ranges for which the single turning points occur. Lower values of mass flux shift the frequency bands to higher values (and vice versa). The linear relationship, evident in figure 7, between ω and M_b is changed only very slightly. This is shown in figure 8 where the

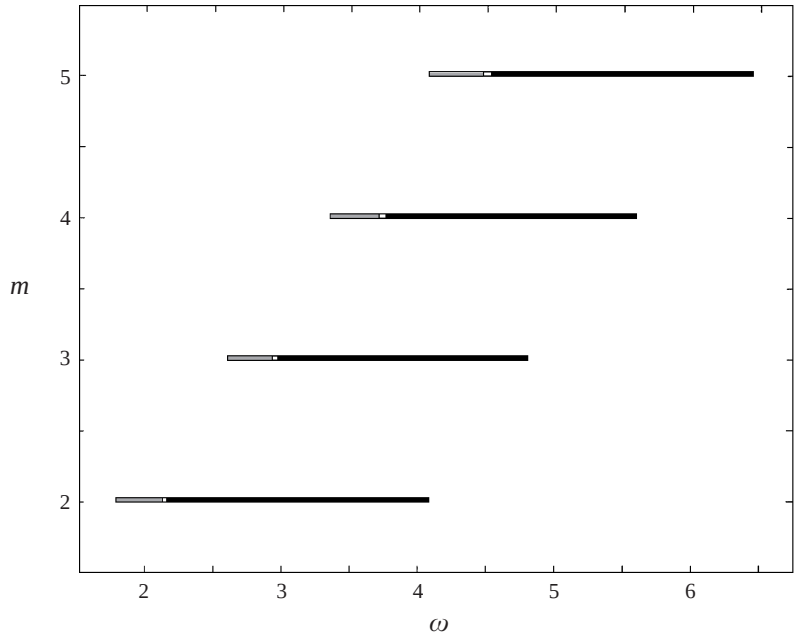

FIGURE 6. Frequency ranges for which there exists a single cut-on mode. Frequencies which produce a single turning point are shown by the grey lines, and frequencies for which the mode is cut on along the entire length of the duct are shown by the black lines. Two turning points occur in the short intermediate-frequency range. To the left of the grey lines all modes are cut off, and to the right of the black lines there are at least two cut-on modes at some point along the duct. ($M_x^f = 0.4015$.)

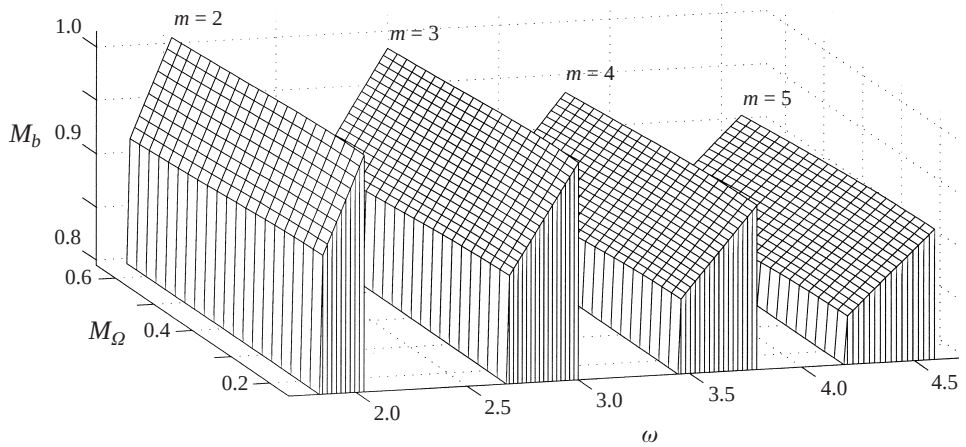

FIGURE 7. Solution planes which satisfy the resonance condition $|M| = 1$. Frequency ranges correspond to the case of a single cut-on mode, with a single turning point at some axial location. ($M_x^f = 0.4015$.)

gradients of the resonance planes for $M_x^f = 0.3089$ and $M_x^f = 0.4324$ are almost the same, and the planes are almost coincident where the frequency ranges overlap.

The matching of phases in the resonance condition (63) is satisfied by the set of values of ε given in (64). Figure 9 shows the values of ε which satisfy this condition

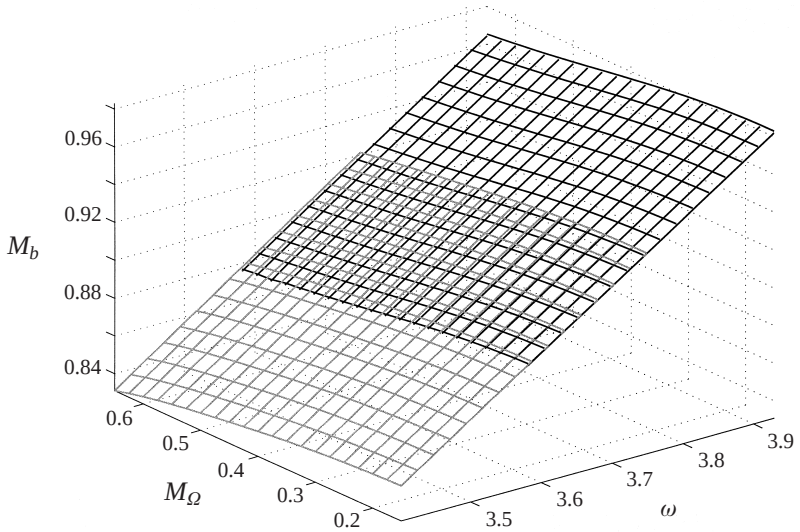

FIGURE 8. Effect of changes in axial mass flux on the resonance planes for $m = 4$. Black mesh is when $M_x^f = 0.3089$ and grey mesh is when $M_x^f = 0.4324$.

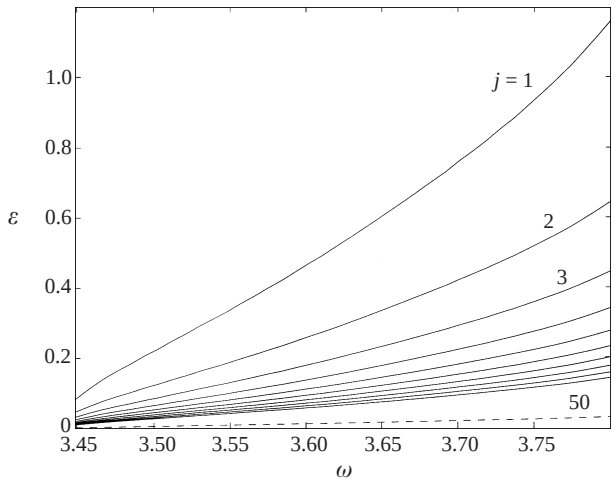

FIGURE 9. Values of ε which match the phase of M in order to satisfy the resonance condition exactly, from (64). $m = 4$, $M_\Omega = 0.4$. Solid lines are for $j = 1, \ldots 10$, dashed line is for $j = 50$.

for the case when $m = 4$, $M_\Omega = 0.4$. It can be seen that for larger values of ε there are rather few discrete frequencies within the practical range for which the resonance condition is completely satisfied. As ε decreases, however, resonance is seen to occur at many more frequencies. From these results it is suggested that for larger values of ε the occurrence of resonance would be reduced, but for aerodynamic reasons aeroengine ducts are always likely to have small values of ε, and so resonance would be likely to occur over a wide range of frequencies.

These results can be extended to include the other cases of reflection due to double turning points, and reflection at the open end of the duct. In the double turning point case energy can 'leak' across the cut-off region, because, although a single

cut-off mode carries precisely zero energy, two cut-off modes propagating in opposite directions lead to a non-zero cross-term in the time-average energy flux. An expression for the reflection coefficient at the turning point nearest to the fan can be derived by considering an inner region around each turning point. In each inner region the wave amplitude $A_0(X)$ satisfies Airy's equation in the same way as for the case of a single turning point, giving the expression

$$R = \frac{K + \mathrm{e}^{\mathrm{i}\pi/2}}{1 + K\mathrm{e}^{\mathrm{i}\pi/2}}, \tag{67}$$

with

$$K = \frac{1}{4}\left(\frac{1 - S\mathrm{e}^{\mathrm{i}\pi/2}}{S + \mathrm{e}^{-\mathrm{i}\pi/2}}\right)\exp\left(\frac{2\mathrm{i}\omega}{\varepsilon}\int_{X_1}^{X_2}\frac{\sigma(y)}{C_0(y)(1 - M_x(y)^2)}\mathrm{d}y\right), \tag{68}$$

where S is the reflection coefficient at the open end of the duct, and the turning points are located at X_1 and X_2 (i.e. the cut-off region is between $X = X_1$ and X_2). Since σ is purely imaginary in a cut-off region this shows how the energy flux across the cut-off region decreases exponentially with the length of the region.

If the cut-off region between the two turning points is long enough, then the behaviour is very similar to that of the single turning point case. However, as the length of the cut-off region decreases more energy is able to leak across, and the behaviour becomes comparable to the completely cut-on case. When a mode is cut on all the way from the inlet to the fan, the upstream-propagating mode must be reflected at the open end of the duct with a particular (complex) reflection coefficient in order for resonance to occur. The reflection coefficients at the end of a cylindrical duct carrying mean flow have been obtained using the Wiener–Hopf technique (as in Levine & Schwinger 1948; Homicz & Lordi 1975; and Peake 1995), and are given in Appendix A. (Note that the slowly varying intake is assumed to be parallel at the intake in order to be able to determine analytical expressions for these coefficients.) Since we consider a thin leading edge at the inlet lip of the duct no vorticity waves are generated from the scattering of the incident acoustic wave. In practice, however, vorticity generation due to separation at the lip may be induced, which in turn may generate an upstream-propagating wave when it is incident at the fan. However, the acoustic resonance described here is able to account for acoustic resonance phenomena observed in practice. Figure 10 shows the magnitude of the reflection coefficients for the velocity potential in the frequency range where a single mode is cut on all along the duct. It is seen that the reflection coefficients have magnitude less than unity, and decrease rapidly with increasing frequency. Hence, the existence of pure acoustic resonance relies on the energy which is lost at the open end of the duct being replaced by energy extracted from the fan and mean flow across the actuator disc to sustain it. Therefore it is found that resonance occurs for a much smaller range of parameters than for the single turning point case. Parameter ranges where the resonance condition is found to be satisfied for $m = 5$ are shown in figure 11. In this case higher values of M_b and M_Ω are required in order to give rise to resonance compared to the case of reflection at a turning point.

So far it has been assumed that the swirling-flow region extends indefinitely downstream of the fan. In fact, in real systems, this region is foreshortened by the presence of a stator (a row of stationary blades) which acts to straighten the exit flow. This system can be modelled by two actuator discs to represent the fan and the stator. This divides the duct into three separate flow regions: regions 1 and 2 are as for the single actuator disc model, except that the region of swirling flow (region 2) is now

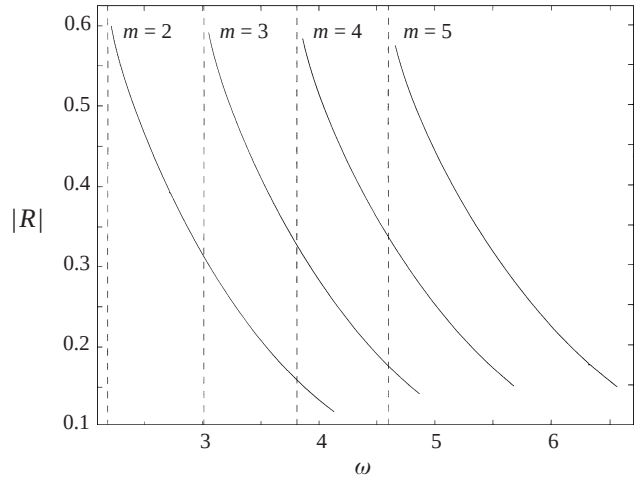

FIGURE 10. Modulus of reflection coefficients for the velocity potential at the open end of the duct in the frequency range where there is a single mode cut on along the entire length of the duct. ($r_t = 1.2881, M_x^l = 0.3900$.) Dashed vertical lines correspond to the cut-off frequency for each m.

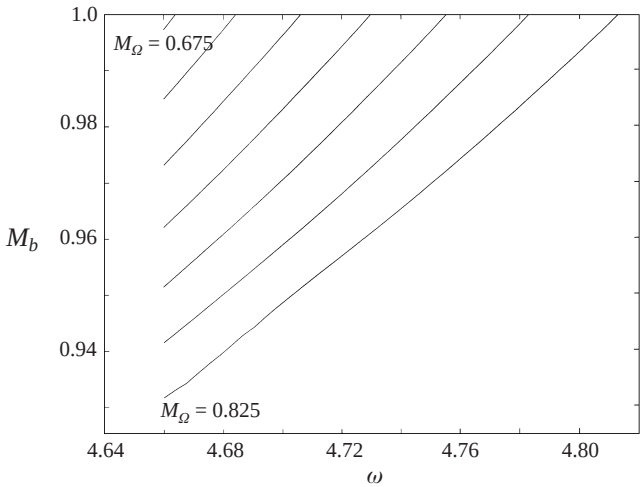

FIGURE 11. Parameters satisfying the resonance condition when $m = 5$ and when the up-stream-propagating mode is reflected at the open end. Lines correspond to different values of M_Ω from 0.675 to 0.825 in steps of 0.025. ($M_x^l = 0.3900, M_x^f = 0.4015$.)

confined to a finite length L of the duct, where L is the gap between the fan and the stator. Upstream-propagating modes are now also assumed to be present in this region. In the third flow region, behind the stator there is uniform axial steady flow and zero swirl with downstream-propagating acoustic and vorticity perturbations. The formulation of this problem is outlined in Appendix B.

The boundary condition imposed by the stator is found to have little significant effect on the results obtained for the fan-only model. This can be seen in figure 12, where values of M_b which satisfy the resonance condition have been calculated for different values of L. This figure is for $m = 5$ and $M_\Omega = 0.38$, and shows that the fan–stator gap has to be very small before any real differences occur. For certain parameter ranges, however, a set of solutions, not present in the results from the

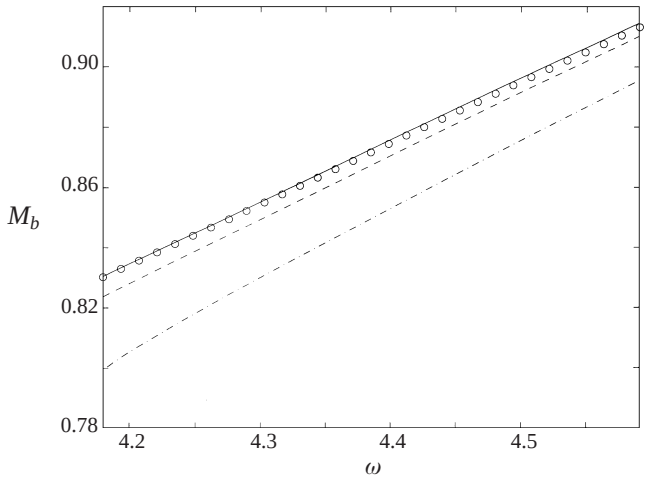

FIGURE 12. Effect of presence of stator for $m = 5$, $M_\Omega = 0.38$, $M_x^f = 0.4015$. Circles denote the results from the single actuator disc model. For the double actuator disc model: solid line: $L = 0.375$, dashed line: $L = 0.25$, dash-dot line: $L = 0.125$.

fan-only model, is found to exist. Figure 13 is a plot of $(\omega, M_b, \log|M|)$ for $m = 2$, $M_\Omega = 0.38$ which shows the two families of solutions. At values of M_b close to 0.9 we see the 'high-speed' resonance observed in the single actuator disc results. In addition to this there is another set of lower values of M_b which satisfy the resonance condition when the stator is introduced. Figure 14 shows values of M_b satisfying the resonance condition for different values of L. It is seen that, as the fan–stator gap increases, the frequency range over which this 'low-speed' resonance occurs narrows. This set of resonance solutions is found to disappear for values of L greater than about 2.0.

6. Discussion

A theoretical model has been developed to study the existence of pure acoustic resonance in aeroengines. The model incorporates a slowly varying duct to represent the intake and includes a swirling-flow region behind the fan, with the fan modelled by an actuator disc.

Slow variations in the cross-sectional area are shown to give rise to turning points in the intake where an acoustic mode changes from being purely cut on to cut off, and vice versa. Discrete bands of frequency for which there is a single cut-on mode at the fan and a single turning point at some location along the duct occur, and the frequency ranges vary with circumferential mode number m. It has been shown that swirling flow behind the fan can cut off acoustic modes which are cut on upstream of the fan, and gives rise to the possibility of the incident cut-on mode being reflected at the fan face. If there is a turning point upstream, then an upstream-propagating mode is totally reflected at this point. For special parameter combinations, multiple reflection of acoustic modes between a turning point and the fan can occur, thus trapping acoustic modes within the duct, leading to pure acoustic resonance.

Two families of parameters which satisfy the condition for resonance were found. The first set of solutions occurs for fairly high values of fan rotational Mach number M_b, and exists with or without the presence of a stator row behind the fan. This set of solutions is largely independent of the fan–stator gap. Conversely, the second set

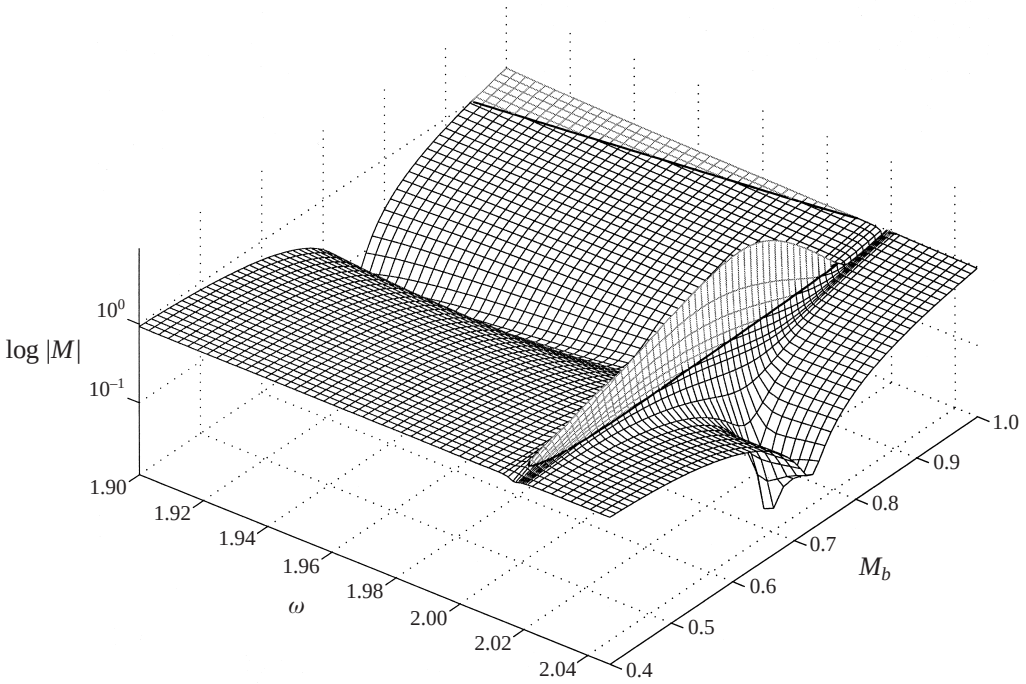

FIGURE 13. Plot of $\log|M|$ as a function of ω and M_b for $m = 2$, $M_\Omega = 0.38$, $M_x^f = 0.4015$. Values of $|M| < 1$ are black lines and values of $|M| > 1$ are grey lines. The resonance condition is satisfied by parameters on the bold black line dividing the two regions.

of solutions is found to occur only when there exists a finite gap between the fan and the stator row. In this case the resonance condition is satisfied for smaller values of M_b, and disappears when the gap exceeds some critical value.

The results shown are very general, in that no relationship between fan speed, swirl Mach number and axial mass flux has been assumed. In practical cases there would be some relationship between M_b, M_Ω and M_x (for instance the camber angle of the fan blades plays a role in the degree of swirl generated behind the fan and the mass flow rate is related to fan speed). For real test cases these relationships would be identified from measured data, and would depend on the particular fan and duct under investigation. Given this information resonance conditions could then be expressed solely in terms of, say, fan speed (M_b) and frequency, thus reducing the number of parameters in the problem. In the general form, however, it is possible to identify cases where the occurrence of acoustic resonance in the duct might be suppressed. This could be achieved by identifying the 'best' duct shape to minimize the effect of the turning points, or conceiving in what way the operating conditions could produce a (M_b, M_Ω, M_x) relationship which lies away from the resonance planes.

Only hard-walled ducts give rise to the occurrence of turning points, so that if the duct is lined completely with an acoustic liner the mechanism for reflection of acoustic waves at a turning point is removed, leaving only reflection at the open end of the duct as a means of generating acoustic resonance. However, it is generally impractical to line the whole of an aeroengine intake duct, but lining a section of the intake may have some attenuation effect on the resonant acoustic modes.

This work is the first step towards understanding a physical mechanism which

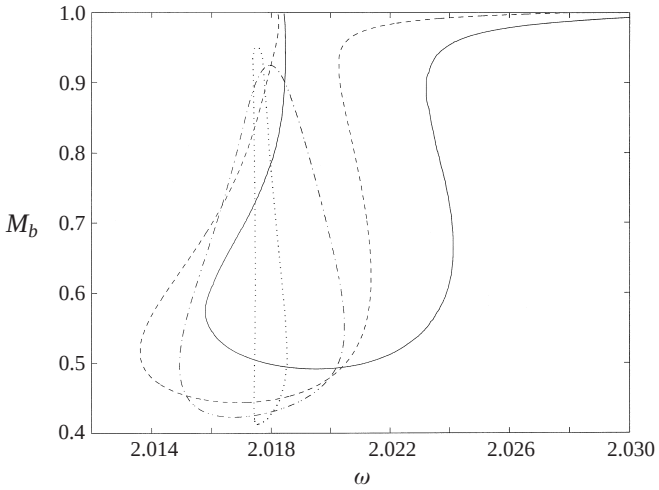

FIGURE 14. Parameter curves satisfying the resonance condition which arise from the inclusion of the stator in the model. $m = 2$, $M_\Omega = 0.38$, $M_x^f = 0.4015$. Solid line: $L = 0.25$, dashed line: $L = 0.375$, dash-dot line: $L = 0.5$, dotted line: $L = 1.0$.

could be associated with the onset of acoustic instabilities in aeroengine intakes, which can generate significant practical problems with the advent of the increasingly wider range of conditions over which aeroengines are required to operate. It has been shown that pure acoustic resonance, arising from the coupling of the intake flow, fan motion and swirling flow downstream of the fan, can be sustained in the inlet duct, and we believe that this may lead to the onset of instabilities.

The work described in this paper is supported by a research grant from EPSRC, reference GR/L80317. The authors would also like to acknowledge useful discussions with Dr A. B. Parry and R. V. Brooks.

Appendix A. Reflection coefficients at open end of duct

Consider an incident cut-on mode which propagates upstream in a cylindrical duct of radius r_t, carrying a uniform axial mean flow with Mach number M_x. At the open end the incident potential field is given by

$$\phi_i = \exp(\mathrm{i}\omega t - \mathrm{i}m\theta - \mathrm{i}k_{mn}^- x) J_m(j'_{mn} r/r_t), \tag{A 1}$$

where j'_{mn} is the nth zero of $J'_m(x)$ (the prime denoting differentiation with respect to argument) and the axial wavenumber k_{mn}^- is defined by

$$k_{mn}^- = \frac{-k_0 M_x - \sqrt{k_0^2 - j'^2_{mn}\beta^2/r_t^2}}{\beta^2}, \tag{A 2}$$

where $\beta^2 = 1 - M_x^2$ and $k_0 = \omega/C_0$.

The field scattered by the lip is

$$\phi = \sum_{s=1}^{N} R_s \exp(\mathrm{i}\omega t - \mathrm{i}m\theta - \mathrm{i}k_{ms}^+ x) J_m(j'_{mn} r/r_t), \tag{A 3}$$

with

$$k_{ms}^{+} = \frac{-k_0 M_x + \sqrt{k_0^2 - j_{ms}'^2 \beta^2 / r_t^2}}{\beta^2}, \qquad s = 1, \ldots N, \tag{A 4}$$

where N is the highest-order radial mode to be cut on. This problem was first solved by Levine & Schwinger (1948), and further work since then has included Homicz & Lordi (1975) and Peake (1995). The results presented in this appendix can be obtained by a straightforward manipulation of equation (11) in Peake (1995).

The reflection coefficients R_s are given by

$$R_s = \frac{\mathscr{K}^{+}(k_{ms}^{+})\mathscr{K}^{-}(k_{mn}^{-}) j_{ms}'^2 [\gamma^{+}(k_{ms}^{+})]^2 [\gamma^{-}(k_{mn}^{-})]^2 J_m(j_{mN}')}{(k_{ms}^{+} - k_{mn}^{-})(m^2 - j_{ms}'^2)(k_{ms}^{+}\beta^2 + M_x k_0) J_m(j_{ms}')}, \tag{A 5}$$

where

$$[\gamma^{\pm}(k)]^2 = \beta^2 \left[k + \frac{M_x k_0}{\beta^2} \pm \frac{k_0}{\beta^2} \right], \tag{A 6}$$

$$\mathscr{K}^{\pm}\left(k - \frac{M_x k_0}{\beta^2} \right) = \frac{\mathscr{J}^{\pm}(k) \prod_{s=1}^{N} (k - k_{ms}^{\mp})}{(k \pm \mathrm{i})^{N-1/2} (-2 r_t \beta)^{1/2} (k \pm k_0/\beta^2)}, \tag{A 7}$$

$$\mathscr{J}^{\pm}(k) = \sqrt{\mathscr{J}(k)} \exp\left[\pm \frac{1}{2\pi \mathrm{i}} \int_{-\infty}^{\infty} \frac{\ln \mathscr{J}(\xi)}{\xi - k} \mathrm{d}\xi \right], \tag{A 8}$$

$$\mathscr{J}(k) = \frac{(k^2+1)^N K_m'(\tilde{\gamma} r_t) I_m'(\tilde{\gamma} r_t)[-2 r_t \beta \sqrt{k^2+1}]}{\prod_{s=1}^{N} (k - k_{ms}^{-})(k - k_{ms}^{+})}, \tag{A 9}$$

$$\tilde{\gamma} = \beta \sqrt{k^2 - \frac{k_0^2}{\beta^4}}, \tag{A 10}$$

and the integral in (A 8) is to be interpreted as a Cauchy principal value. The square root in (A 10) is defined by inserting branch cuts in the complex k-plane running from $\pm k_0/\beta^2$ to infinity through the upper and lower half-planes respectively, and with $\tilde{\gamma}$ real and positive as $k \to \pm\infty$. The relationship between the functions $\mathscr{K}(k)$ and $\mathscr{J}(k)$ has been chosen in such a way as to facilitate numerical evaluation of the integral in (A 8), so that for instance $\mathscr{J}(\xi) \to 1$ as $\xi \to \pm\infty$ and $\mathscr{J}(\xi)$ is free of zeros on the real ξ-axis.

Appendix B. Twin actuator disc model for rotor–stator pair

For the twin actuator disc model, two actuator discs are placed within the duct to represent the fan (or rotor) and the stator. This divides the duct into three flow regions. In the first region, the slowly varying intake, the flow field is the same as for the single actuator disc model. In the second, swirling flow, region behind the fan, the flow field is derived from the same potential functions as for the single actuator disc case. This is expressed in terms of four sets of unknown constants $A_n^{p^+}, A_n^{p^-}, A_n^{l}$ and A_n^{r}, to represent upstream- and downstream-propagating acoustic-type modes and the

two branches of the vorticity-dominated modes. Thus at the fan location ($x = x_f$)

$$u_r^{(2)} = \sum_\tau \sum_{n=1}^{\infty} A_n^\tau \left\{ \frac{\partial \phi_n^\tau}{\partial r} + R_n^\tau \right\}, \tag{B 1}$$

$$u_\theta^{(2)} = \sum_\tau \sum_{n=1}^{\infty} A_n^\tau \left\{ \frac{-\mathrm{i}m\phi_n^\tau}{r} + T_n^\tau \right\}, \tag{B 2}$$

$$u_x^{(2)} = \sum_\tau \sum_{n=1}^{\infty} A_n^\tau \{-\mathrm{i}k_n^\tau \phi_n^\tau\}, \tag{B 3}$$

$$p^{(2)} = \sum_\tau \sum_{n=1}^{\infty} A_n^\tau \{-\mathrm{i}\Lambda_n^\tau \phi_n^\tau\}, \tag{B 4}$$

with a factor $\exp\{\mathrm{i}(\omega t - m\theta)\}$ understood throughout, and τ denoting one of p^+, p^-, l and r. $\sum_\tau$ is used to denote the sum over the modes p^+, p^-, l and r. At the stator location ($x = x_s$) the solutions are as above but multiplied by a factor $\exp(-\mathrm{i}k^\tau L)$, where $L = x_s - x_f$ is the non-dimensional distance between the fan and the stator.

In the third region, behind the stator, the steady flow is purely axial with the same axial Mach number as that just upstream of the fan, and the unsteady flow field consists of downstream-propagating acoustic and vorticity modes. The acoustic field is expressed in terms of the same Bessel functions as appeared in region 1, so that

$$\phi^{(3)} = \sum_{n=1}^{\infty} B_n^d C_m(\alpha_n r) \exp(\mathrm{i}\omega t - \mathrm{i}m\theta - \mathrm{i}k_n^+(x - x_f)). \tag{B 5}$$

The purely convected vorticity field with velocity components (a_x, a_r, a_θ) can also be written in terms of Bessel functions (see Golubev & Atassi 1995). If

$$a_r(r) = AJ_m(\beta r) + BY_m(\beta r), \tag{B 6}$$

where A and B are arbitrary constants, then the boundary conditions $a_r(r_h) = a_r(r_t) = 0$ mean that the radial eigenvalues β must satisfy the relation

$$J_m(\beta r_t)Y_m(\beta r_h) - J_m(\beta r_h)Y_m(\beta r_t) = 0. \tag{B 7}$$

The vorticity field can then be expressed as

$$\begin{aligned}(a_x, a_r, a_\theta) &= \sum_{n=1}^{\infty} (\mathrm{i}A_n^x, A_n^r, A_n^\theta) \left\{ J_m(\beta_n r) - \frac{J_m(\beta_n r_h)}{Y_m(\beta_n r_h)} Y_m(\beta_n r) \right\} \\ &\quad \times \exp(\mathrm{i}\omega t - \mathrm{i}m\theta - \mathrm{i}k_x(x - x_f)) \\ &= \sum_{n=1}^{\infty} (\mathrm{i}A_n^x, A_n^r, A_n^\theta) G_m(\beta_n r) \exp(\mathrm{i}\omega t - \mathrm{i}m\theta - \mathrm{i}k_x(x - x_f)),\end{aligned} \tag{B 8}$$

where $k_x = \omega / U_0^f$ is the convected wavenumber. However, the vorticity field must satisfy $\nabla \cdot \boldsymbol{a} = 0$, so that one of the constants can be eliminated through setting

$$a_\theta = -\frac{-\mathrm{i}r}{m} \left\{ \frac{\partial a_r}{\partial r} + \frac{a_r}{r} - \mathrm{i}k_x a_x \right\}. \tag{B 9}$$

The boundary conditions at the fan are the same as in the single actuator disc

problem (equations (31)–(34)), while the corresponding conditions imposed at the stator are

$$\frac{M_x^f p^{(2)}}{C_0} + \rho_0 u_x^{(2)} = \frac{M_x^f p^{(3)}}{C_0(X_f)} + D_0(X_f) u_x^{(3)}, \tag{B 10}$$

$$u_r^{(2)} = u_r^{(3)}, \tag{B 11}$$

$$\frac{p^{(2)}}{\rho_0} + C_0\{M_x^f u_x^{(2)} + rM_\Omega u_\theta^{(2)}\} = \frac{p^{(3)}}{D_0(X_f)} + C_0(X_f) M_x^f u_x^{(3)}, \tag{B 12}$$

$$u_\theta^{(3)} = 0. \tag{B 13}$$

The eight boundary conditions are transformed into a set of eight matrix equations in the same way as in the single actuator disc example. Manipulation of these equations eliminates the unknown constants $A_n^{p^+}, A_n^{p^-}, A_n^l, A_n^r, B_n^d, A_n^x$ and A_n^r to again leave an expression

$$\boldsymbol{A}^u = \hat{\boldsymbol{M}} \boldsymbol{A}^d, \tag{B 14}$$

which relates upstream- and downstream-propagating acoustic modes at the fan. The necessary condition for resonance is that $|\hat{M}_{11}| = 1$ when there is just one mode cut on.

REFERENCES

Astley, R. J. & Eversman, W. 1981 Acoustic transmission in non-uniform ducts with mean flow, part II. *J. Sound Vib.* **74**, 103–121.

Evans, D. V., Levitin, M. & Vassiliev, D. 1994 Existence theorems for trapped modes. *J. Fluid Mech.* **261**, 21–31.

Evans, D. V. & Linton, C. M. 1991 Trapped modes in open channels. *J. Fluid Mech.* **225**, 153–175.

Evans, D. V. & Linton, C. M. 1994 Acoustic resonance in ducts. *J. Sound Vib.* **173**, 85–94.

Eversman, W. & Astley, R. J. 1981 Acoustic transmission in non-uniform ducts with mean flow, part I. *J. Sound Vib.* **74**, 89–101.

Golubev, V. V. & Atassi, H. M. 1995 Aerodynamic and acoustic response of a blade row in unsteady swirling flow. In *Proc. First Joint CEAS/AIAA Aeroacoustics Conference, Munich, Germany*, pp. 167–176.

Golubev, V. V. & Atassi, H. M. 1996 Sound propagation in an annular duct with mean potential swirling flow. *J. Sound Vib.* **198**, 601–616.

Golubev, V. V. & Atassi, H. M. 1998 Acoustic-vorticity waves in swirling flows. *J. Sound Vib.* **209**, 203–222.

Homicz, G. & Lordi, J. A. 1975 A note on the radiative directivity pattern of duct acoustic modes. *J. Sound Vib.* **41**, 283–290.

Horlock, J. H. 1978 *Actuator Disk Theory. Discontinuities in Thermo-fluid Dynamics.* McGraw-Hill.

Howe, M. S. & Liu, J. T. C. 1977 The generation of sound by vorticity waves in swirling duct flows. *J. Fluid Mech.* **81**, 369–383.

Kerrebrock, J. L. 1977 Small disturbances in turbomachine annuli with swirl. *AIAA J.* **15**, 794–803.

Khorrami, M. R. 1991 A Chebyshev spectral collocation method using a staggered grid for the stability of cylindrical flows. *Intl J. Numer. Meth. Fluids* **12**, 825–833.

Levine, H. & Schwinger, J. 1948 On the radiation of sound from an unflanged circular pipe. *Phys. Rev.* **73**, 383–406.

Linton, C. M. & McIver, P. 1998 *a* Acoustic resonances in the presence of radial fins in circular cylindrical waveguides. *Wave Motion* **28**, 99–117.

Linton, C. M. & McIver, P. 1998 *b* Trapped modes in cylindrical waveguides. *Q. J. Mech. Appl. Maths* **51**, 389–412.

Nayfeh, A. H. & Telionis, D. P. 1973 Acoustic propagation in ducts with varying cross section. *J. Acoust. Soc. Am.* **54**, 1654–1661.

NAYFEH, A. H., SHAKER, B. S. & KAISER, J. E. 1980 Transmission of sound through nonuniform circular ducts with compressible mean flows. *AIAA J.* **18**, 515–525.

PARKER, R. 1966 Resonance effects in wake shedding from parallel plates: some experimental observations. *J. Sound Vib.* **4**, 62–72.

PARKER, R. 1967 Resonance effects in wake shedding from parallel plates: calculation of resonant frequencies. *J. Sound Vib.* **5**, 330–343.

PARKER, R. & STONEMAN, S. A. T. 1989 The excitation and consequences of acoustic resonance in enclosed fluid flow around solid bodies. *Proc. Inst. Mech. Engrs* **203**, 9–19.

PEAKE, N. 1995 On the radiation properties of an asymmetric cylinder. *Wave Motion* **22**, 371–385.

RIENSTRA, S. W. 1999 Sound transmission in slowly varying circular and annular ducts with mean flow. *J. Fluid Mech.* **380**, 279–296.

RIENSTRA, S. W. & HIRSCHBERG, A. 1999 An introduction to acoustics. *Rep.* IWDE 99-02, TU Eindhoven.

TAM, C. K. W. & AURIAULT, L. 1998 The wave modes in ducted swirling flows. *J. Fluid Mech.* **371**, 1–20.

WOODLEY, B. M. & PEAKE, N. 1999 *a* Resonant acoustic frequencies of a tandem cascade. Part 1. Zero relative motion. *J. Fluid Mech.* **393**, 215–240.

WOODLEY, B. M. & PEAKE, N. 1999 *b* Resonant acoustic frequencies of a tandem cascade. Part 2. Rotating blade rows. *J. Fluid Mech.* **393**, 241–256.